ARTICLE

Bulk Mixing and Decoupling of the Nocturnal Stable Boundary Layer Characterized Using a Ubiquitous Natural Tracer

A. G. Williams · S. Chambers · A. Griffiths

Abstract Vertical mixing of the nocturnal stable boundary layer (SBL) over a complex land surface is investigated for a range of stabilities, using a decoupling index ($0 < D_{rb} < 1$) based on the 2–50 m bulk gradient of the ubiquitous natural trace gas radon-222. The relationship between D_{rb} and the bulk Richardson number (R_{ib}) exhibits three broad regions: (1) a well-mixed region ($D_{rb} \approx 0.05$) in weakly stable conditions ($R_{ib} < 0.03$); (2) a steeply increasing region ($0.05 < D_{rb} < 0.9$) for "transitional" stabilities ($0.03 < R_{ib} < 1$); and (3) a decoupled region ($D_{rb} \approx 0.9$–1.0) in very stable conditions ($R_{ib} > 1$). D_{rb} exhibits a large variability within individual R_{ib} bins, however, due to a range of competing processes influencing bulk mixing under different conditions. To explore these processes in R_{ib}–D_{rb} space, we perform a bivariate analysis of the bulk thermodynamic gradients, various indicators of external influences, and key turbulence quantities at 10 and 50 m. Strong and consistent patterns are found, and five distinct regions in R_{ib}–D_{rb} space are identified and associated with archetypal stable boundary-layer regimes. Results demonstrate that the introduction of a scalar decoupling index yields valuable information about turbulent mixing in the SBL that cannot be gained directly from a single bulk thermodynamic stability parameter. A significant part of the high variability observed in turbulence statistics during very stable conditions is attributable to changes in the degree of decoupling of the SBL from the residual layer above. When examined in R_{ib}–D_{rb} space, it is seen that very different turbulence regimes can occur for the same value of R_{ib}, depending on the particular combination of values for the bulk temperature gradient and wind shear, together with external factors. Extremely low turbulent variances and fluxes are found at 50 m height when $R_{ib} > 1$ and $D_{rb} \approx 1$ (fully decoupled). These "quiescent" cases tend to occur when geostrophic forcing is very weak and subsidence is present, but are not associated with the largest bulk temperature gradients. Humidity and net radiation data indicate the presence of low cloud, patchy fog or dew, any of which may aid decoupling in these cases by preventing temperature gradients from increasing sufficiently to favour gravity wave activity. The largest temperature gradients in our dataset are actually

A. G. Williams (✉) · S. Chambers · A. Griffiths
Australian Nuclear Science and Technology Organisation, Institute for Environmental Research,
Locked Bag 2001, Kirrawee DC, NSW 2232, Australia
e-mail: Alastair.Williams@ansto.gov.au

associated with smaller values of the decoupling index ($D_{rb} < 0.7$), indicating the presence of mixing. Strong evidence is seen from enhanced turbulence levels, fluxes and submeso activity at 50 m, as well as high temperature variances and heat flux intermittencies at 10 m, suggesting this region of the R_{ib}–D_{rb} distribution can be identified as a top-down mixing regime. This may indicate an important role for gravity waves and other wave-like phenomena in providing the energy required for sporadic mixing at this complex terrain site.

1 Introduction

1.1 Turbulent Mixing in the Nocturnal Stable Boundary Layer (SBL)

In the nocturnal SBL over land, the intensity, extent and evolution of turbulent mixing are controlled and modulated by numerous interacting processes. Although much is understood about SBL behaviour in near-neutral to moderately stable conditions when turbulence is vertically continuous and connected to the surface (i.e. Monin–Obukhov similarity or the local scaling theory of Nieuwstadt (1984) applies), characterization of mixing in the very stable boundary layer (vSBL) remains highly problematic. Strongly stratified flow that develops due to clear-sky nocturnal longwave cooling of the ground in the presence of low wind speeds frequently exhibits turbulent mixing that is intermittent in nature (Businger 1973; Howell and Sun 1999; Mahrt 1999; Van de Wiel et al. 2002a,b, 2003; Mahrt and Vickers 2002, 2006; Banta et al. 2007; Ohya et al. 2008). If winds are very weak, cooling by radiative flux divergence in the lowest 50 m (usually ignored) can become comparable in magnitude to sensible heat-flux divergence, especially in the early evening and when fog is present (Van de Wiel et al. 2003; Ha and Mahrt 2003; Sun et al. 2003). In calm conditions, the surface-based mixed layer can become very thin indeed (<30 m) and completely decoupled from the atmosphere above (Smedman 1988; Mahrt and Vickers 2006; Banta et al. 2007; Mahrt 2011). If the flow aloft has a tendency to accelerate as a result of this decoupling, together with a large-scale pressure gradient (forming a low-level jet), the growing shear may then generate new turbulence and mixing, causing the SBL to temporarily re-couple with the deeper layer (Businger 1973; Nappo 1991; Van de Wiel et al. 2002a,b, 2003; Acevedo and Fitzjarrald 2003). The vSBL is also known to be highly sensitive to even minor variations in local surface roughness, thermal properties and terrain inclination, generating local density currents, meandering motions, secondary circulations, microfronts and sudden flow perturbations (e.g. Nappo 1991; Mahrt et al. 2001; Acevedo and Fitzjarrald 2003; Mahrt 2010a). Together with propagating solitary and internal gravity waves that can transport remotely-generated energy horizontally and vertically into the local area, these "submeso" disturbances can sporadically initiate strong turbulent mixing despite the stable stratification (Hunt et al. 1985; King et al. 1987; Poulos et al. 2002; Sun et al. 2004; Mahrt 2010b). In fact, at very low wind speeds, it may be that turbulence is generated predominantly by the submeso motions, and its relationship to the mean flow becomes weak (Mahrt 2011; Sun et al. 2012). Turbulence that is primarily generated aloft (e.g. by shear associated with a low-level jet or gravity waves) is termed "upside-down" mixing, and may be partially or completely detached from the surface and confined to thin elevated layers (Ohya et al. 1997; Ohya 2001; Mahrt et al. 1998; Cuxart

et al. 2000; Ha and Mahrt 2001; Mahrt and Vickers 2002; Conangla and Cuxart 2006). In such cases, the traditional concept of a boundary layer breaks down altogether (Mahrt 1999).

Progress has been made in recent years in classifying mixing/scaling regimes incorporating the vSBL (Holtslag and Nieuwstadt 1986; Ohya et al. 1997; Mahrt et al. 1998; Mahrt 1998, 1999; Van de Wiel et al. 2002a,b, 2003; Zilitinkevich et al. 2008; Sorbjan and Grachev 2010), developing similarity formulations applicable over a wider range of stabilities (e.g. Sorbjan 2006a, 2008; Sorbjan and Grachev 2010) and dealing with data analysis problems associated with submeso motions, non-stationarity and self-correlation (Vickers and Mahrt 2003, 2006; Klipp and Mahrt 2004; Sorbjan 2006b; Mahrt 2011). However, the complexity of the numerous processes active in the vSBL, as well as the difficulty of predicting which of them will be operating at any one time and location, has meant that the goal of a robust generalized characterization of the vertically integrated behaviour of the SBL under a wide range of conditions has yet to be realised, and remains a topic of intense interest within the research community. The failure of numerical weather, climate and dispersion models to represent SBL characteristics adequately within their finite grid structure leads to a range of problems, including inadequate predictions of surface temperature, fog, dew/frost and pollution levels (e.g. Mahrt 1998; Cuxart et al. 2006; Price et al. 2011).

One approach to this difficult subject in an integrated way is to first recognize that profiles of the internal thermodynamic variables (primarily temperature and wind) play a direct and central role in both the forcing and modulation of turbulence in the SBL. Controlled externally through source and sink functions that are highly complex in time and space, they provide the immediate environment for turbulence but are in turn also strongly modified by its presence. Because these profiles are closely involved at "both ends" of the mixing process, it can be difficult to interpret them when attempting to separate the driving of turbulent mixing from its ultimate outcomes. In contrast, changes in the distribution of a simple passive scalar can provide direct and unambiguous information regarding the outcomes of turbulent mixing, including its strength and vertical extent. Measurements of unreactive trace gases with appropriate properties therefore have the potential to help disentangle complex relationships of cause and effect in the study of atmospheric turbulence, and illuminate previously obscured features of boundary-layer structure.

1.2 A Framework for the Bulk Characterization of Mixing

Turbulence in the SBL is driven primarily by the vertical wind-speed gradient and suppressed by the vertical temperature gradient. We choose to express the balance between these influences using the well-known stability measure known as the bulk Richardson number, viz.

$$R_{ib} = \frac{\dfrac{g}{\theta}\dfrac{\Delta\theta}{\Delta z}}{\left(\dfrac{\Delta U}{\Delta z}\right)^2} = \frac{N_b^2}{S_b^2}, \tag{1}$$

where $\Delta\theta = \theta(z_m) - \theta_s$, $\Delta U = U(z_m)$ are the differences of potential temperature and wind speed across the layer $\Delta z = z_m - z_s$ where z_m is the upper measurement height and z_s corresponds to the surface. N_b and S_b are the bulk Brunt–Väisälä frequency and wind shear, respectively. In this study, the bulk gradients are evaluated across the layer from $z_s = 2$ m to $z_m = 50$ m. In our approach, R_{ib} is considered to precede (establish an environment for) actual mixing, and may then be modified by it. We follow Mahrt and Vickers (2006) and Banta et al. (2007) and others in rejecting the use of the Monin–Obukhov parameter (z/L) as a bulk

stability measure, due to its uncertainty and self-correlation problems at high stabilities (when turbulent fluxes are close to zero). As with Mahrt (2010b), we wish to relate the outcomes of turbulent mixing to a bulk stability measure that is independent of turbulence quantities.

We adopt the tracer difference $\Delta C = C(z_m) - C_s$ across the layer Δz as an unbiased measure of the layer-integrated outcome of the turbulent mixing process. As ΔC depends on the surface concentration (C_s), which, in practice, is influenced by a number of extraneous factors including geographic variations in the surface flux over the air mass fetch history (Chambers et al. 2011), it is important to normalize our measure of bulk mixing appropriately. In this study, we characterize scalar mixing in the SBL using the mass-based decoupling index,

$$D_{rb} = \frac{-\Delta C}{C_s - C_b} \tag{2}$$

where C_b is the "background" concentration in the residual layer above. D_{rb} expresses the degree of decoupling between the surface-based shear-driven mixed layer and the residual layer above, with $D_{rb} = 0$ denoting completely mixed conditions and $D_{rb} = 1$ denoting completely decoupled conditions. In practice, D_{rb} can take values below zero and above one, corresponding to 50 m concentrations that are greater than C_s and less than C_b, respectively. Such cases are relatively rare, however, and are interpreted as corresponding to non-stationary conditions. In this study, we allow a small margin of ± 0.2 around the "acceptable" range of values for D_{rb} [$-0.2 < D_{rb} < 1.2$] and disregard all data points falling outside this range.

We consider R_{ib} and D_{rb} together to represent a two-dimensional cause-effect framework for the characterization of bulk mixing in the SBL.

1.3 Atmospheric Radon as a Tracer for Vertical Mixing Over Land

We use the naturally occurring, radioactive noble gas radon (^{222}Rn) to represent the bulk mixing characteristics of passive scalars in the nocturnal SBL. Radon's salient characteristics as a tracer in ABL mixing studies have been discussed in Williams et al. (2011) and Chambers et al. (2011). As its origin is almost exclusively soils and rocks at the land surface (Wilkening and Clements 1975; Turekian et al. 1977), atmospheric radon is ubiquitous with a relatively modest spatial variability in source strength over ice-free terrestrial surfaces (typically 15–25 mBq m^{-2} s^{-1}; Turekian et al. 1977; Lambert et al. 1982). For the purposes of vertical mixing studies, temporal source variations can be considered to be negligible on diurnal time scales (Israelsson 1978; Gogolak and Beck 1980; Griffiths et al. 2010). Furthermore, atmospheric radon's only significant sink is radioactive decay, and its half-life of 3.8 days is long compared with turbulent time scales but sufficiently short to ensure that a concentration decrease is maintained between the surface and the free troposphere that is typically two orders of magnitude (Liu et al. 1984; Williams et al. 2011).

In contrast to the use of single-height observations of radon and its progeny to investigate atmospheric stability and dilution effects near the ground, studies reporting vertical radon variations are rare (see reviews in Chambers et al. 2011 and Williams et al. 2011). Although radon profiles correlate well with atmospheric mixing (Pearson and Moses 1966; Hosler 1969; Williams et al. 2011), the practical difficulties of measuring high-resolution (multi-height) profiles of radon make long-term measurements unrealistic. A sustainable and productive compromise is the two-point gradient approach, in which the radon concentration difference, ΔC, is measured across an atmospheric layer adjacent to the surface (Druilhet et al. 1980; Ussler et al. 1994; Chambers et al. 2011). Vertical differencing removes or reduces background signals associated with horizontal advection and fetch-related source variations, and compared with more common methods, the use of radon gradients for deriv-

ing vertical mixing measures is simpler and less restricted to ideal surface or meteorological conditions (Butterweck et al. 1994). Finally, due to radon's 3.8 day half-life, there is no need to account for radioactive decay in hourly gradient observations (Hosler 1969).

1.4 Outline

This study represents an attempt to characterize and interpret the integrated behaviour of vertical mixing and decoupling in the SBL at a complex mid-latitude continental location over a range of stabilities, using radon as a ubiquitous natural trace gas to provide a mass-based measure of bulk mixing that is independent of the thermodynamic properties of the layer of interest. Following a description of the site characteristics, available measurements and data analysis techniques in Sect. 2, we begin our analysis of results by examining general characteristics of the relationship between our chosen bulk measures of stability (R_{ib}) and mixing (D_{rb}) in Sect. 3.1. As it will be seen that R_{ib} and D_{rb}, although connected, are by no means dependent, the interpretation of position in $R_{ib}-D_{rb}$ space and how it relates to vertical location within the SBL is discussed in Sect. 3.2. With this interpretation in mind, we then consider how measures of external influences (Sect. 3.3) and internal turbulence quantities (Sect. 3.4) are represented in $R_{ib}-D_{rb}$ space. In Sect. 4, we summarize our findings by considering archetypal SBL types and how they map into different regions of $R_{ib}-D_{rb}$ space.

2 Location and Measurements

2.1 Site Characteristics

In late 2005 a pair of detectors was installed at the Australian Nuclear Science and Technology Organisation (ANSTO) headquarters at Lucas Heights (34°03′S, 150°59′E) for the continuous hourly monitoring of atmospheric radon concentrations at two heights. Lucas Heights is 30 km south-west of Sydney and 18 km from the coast. Major geographical features are shown in Fig. 1. Being at the southern edge of the Sydney metropolitan area, surface land use in the area is a mixture of residential suburbs (mainly to the east and north), light industry (ANSTO and the waste management centre directly to its north-west) and natural vegetation (most of the southern semicircle). The local topography is fairly complex, with changes in elevation on the order of 100–150 m within 1–2 km of the site (Fig. 1b). There is no large-scale orography nearby, however, and so the site topography could be described as similar to the region of small hills studied in COLPEX (Price et al. 2011). ANSTO itself is atop a broad ridge, with significant gullies close by to the east and south. In the direct vicinity of the measurement site, fetch conditions are highly heterogeneous. Immediately (30–80 m) to both the east and west there are low (1–2 storey) buildings; 100 m to the south there is natural eucalypt forest; and to the north, the tower is adjacent to grassed playing fields. The tower's location near the southern edge of the Lucas Heights site, together with the fact that the prevailing nocturnal wind direction is in the sector south-south-east to west-south-west, however, results in a large proportion of measurements being representative of relatively unobstructed air approaching from the extended fetch of natural vegetation to the south (Fig. 1), where there is a series of ridges and gullies.

2.2 Tower and Surface Measurements

Radon sampling at the Lucas Heights site was conducted on a 50-m tower with inlets positioned at 2 and 50 m above ground level (a.g.l.). Details of the radon measurement principle,
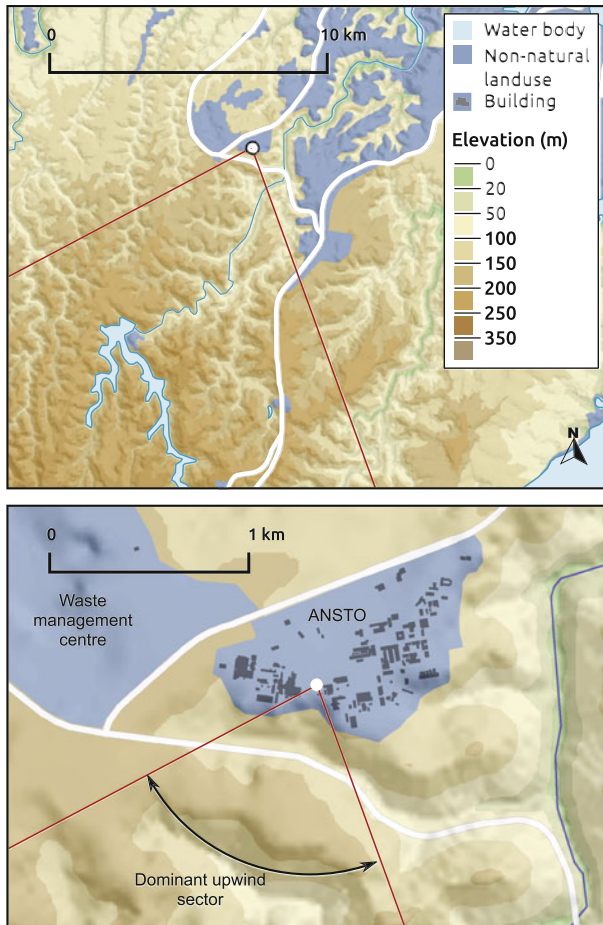
Fig. 1 (*Upper panel*) Regional geographical setting and *lower panel* details of the measurement site at the ANSTO, Lucas Heights, Sydney Australia. Prevailing nocturnal wind directions south-south-east to west-south-west are shown with *red lines*. Data sourced from Geoscience Australia (www.ga.gov.au) and the Open Street Map project (www.openstreetmap.org)

sampling and calibration methodology can be found in Chambers et al. (2011). Hourly-mean atmospheric radon concentrations are produced by this technique, with a lower limit of detection (defined as the concentration at which the relative counting error exceeds 30 %) of around 40 mBq m^{-3} for both detectors.

Two three-dimensional (3D) sonic anemometers (Gill WindMaster Pro) recorded 20 Hz wind components and fast response sonic air temperatures at 10 and 50 m a.g.l. on the Lucas Heights tower. Measurements made with the system gain at maximum, indicating the presence of an obstruction in the signal path such as condensation on the transducers, were excluded from the final dataset. Sonic temperature is internally corrected for crosswind contamination.

Given the complexity of the site and the prevalence of submeso motions in the SBL (see Sect. 1), the nocturnal data gathered using the sonic anemometers are expected to contain a significant submeso component. In order to separate turbulent and submeso components

in the statistics derived from the sonic data, variances and covariances were first computed using 2-min linearly detrended data blocks and then averaged back to hourly values to reduce random flux errors. This technique is similar to Klipp and Mahrt (2004). Statistics of the sub-hourly variations were also computed and retained, in order to characterize the strength of submeso motions and intermittency.

Air temperature, relative humidity (Vaisala, HMP45C), wind speed and wind direction (Gill, 2-D windsonic) were recorded at 2, 10 and 50 m a.g.l. on the Lucas Heights tower; incoming shortwave radiation (LI-COR silicon pyranometer) and net radiation (REBS, Q7.1) sensors were mounted at 10 m a.g.l. Other measured quantities included: surface atmospheric pressure, soil moisture, soil temperature, ground heat flux, rainfall and radiative surface temperature. Meteorological measurements were stored on a Campbell CR-1000 data logger as 10-min averages of 20-s readings and later aggregated to hourly values to match the radon and eddy-covariance measurements.

2.3 Data Availability, Constraints and Definitions

Due to periods of maintenance or malfunction, the 2 and 50 m radon detectors were only in simultaneous operation for approximately 2 years and 7 months of the 4-year period 2006–2009. In addition, turbulence data from the sonic anemometers were not used when wind directions were in the range 275–335°, corresponding to the angle subtended by the (substantial) tower structure. For the current study, only nocturnal hours were used (1800–0500, Australian Eastern Standard Time, AEST) with the additional constraints that a stable stratification (positive $\Delta\theta$) should be indicated by both the 2–50 and the 2–10 m temperature differences. Removing all missing data and applying all constraints resulted in a total of 3472 hourly data points (equivalent to 316 nights) available for the final analysis.

A large fraction (around 55 %) of the final dataset sampled the unobstructed fetch from the dominant south-south-east to west-south-west sector. This included a large proportion of the high bulk Richardson number cases (76 % of cases with $R_{ib} > 1$) representing light wind speeds and high surface pressures (weak synoptic flow). The site's ridge top location likely precludes the formation of a deep SBL, due to slow drainage flows into nearby valleys at night in light winds and subsidence conditions. Higher nocturnal wind speeds tended to be associated with a more south-west to west component and lower R_{ib} values. Winds with an easterly component were relatively rare at night, and tended to occur in the early evening. The north-westerly direction is not represented in this dataset, due to the tower obstruction (see above).

Unless otherwise stated, R_{ib}, D_{rb} and all gradients discussed in the analysis correspond to differences between the 2-m and 50-m levels on the Lucas Heights tower. Surface radon concentrations (C_s) correspond to the 2-m level, and "background" (residual layer) radon concentrations (C_b) are estimated as the minimum of all measured radon concentrations in the four hours before sunset (assumed to be 1800 AEST).

3 Results

3.1 Broad Features of the Stability-Mixing Relationship

Figure 2a presents hourly D_{rb} values versus R_{ib} for the entire dataset; also shown are median and quartile values of D_{rb} calculated in logarithmic R_{ib} bins. Three distinct regions are apparent in the distribution:
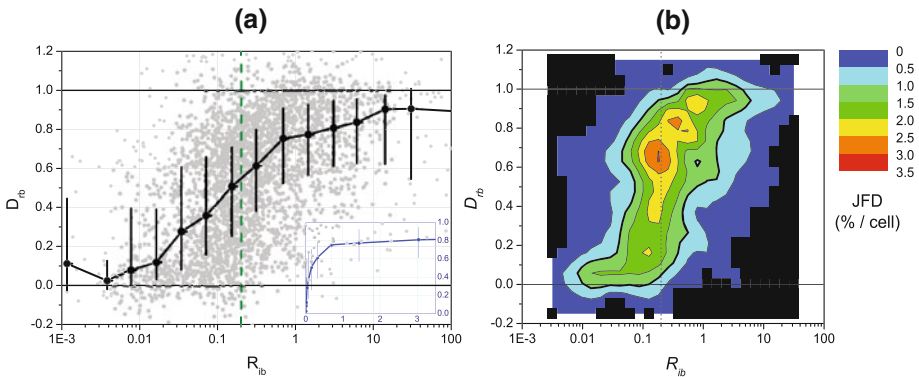
Fig. 2 **a** Hourly D_{rb} values versus R_{ib}, both as a scatter plot (*grey*) and as median and quartile values in logarithmic R_{ib} bins (*black*); *inset* is the median/quartile plot with a linear R_{ib} axis (*blue*); and **b** joint frequency distribution (24 × 24 grid points) of hourly data in $R_{ib}-D_{rb}$ space. Grid squares containing less than four data points are masked out in *black*. In both plots, *vertical dashed lines* indicate the (nominal) value of the critical bulk Richardson number ($R_{ib} \approx 0.2$)

1. A well-mixed region ($D_{rb} \approx 0.05$) in weakly stable conditions ($R_{ib} < 0.03$).
2. A steeply increasing region ($0.05 < D_{rb} < 0.9$) for "transitional" stabilities ($0.03 < R_{ib} < 1$).
3. A decoupled region ($D_{rb} \approx 0.9$–1.0) in very stable conditions ($R_{ib} > 1$).

The logarithmic binning of R_{ib} results in a broader, more gradually increasing, relationship than is apparent in the scatter plot. This is due to the natural bounds on the D_{rb} values at both zero and one, which leads to strongly skewed distributions close to both extremes (see quartile ranges in Fig. 2a). Such biases are removed by binning the distribution in both dimensions, and Fig. 2b presents the joint frequency distribution (JFD) of hourly data in $R_{ib}-D_{rb}$ space (number of data points falling into a particular grid cell, expressed as a percentage of the total data points). This presents a clearer and less biased interpretation of the dataset than the R_{ib} binning shown in Fig. 2a, and also introduces a useful framework for the bivariate analysis presented later.

The location of maximum data concentration in the JFD is likely to be affected both by site characteristics and the upper measurement height. In particular, the maximum would be expected to shift left or right (R_{ib} dependence) according to the predominance of stability types encountered at a particular site, and up or down (D_{rb} dependence) according to the height of the upper measurement relative to typical boundary-layer depths (normalized height, z_m/h). It is not intuitively obvious, however, whether the main *shape* of the JFD would change from site to site, or indeed over the course of a typical night. For example, it is unclear whether the three regions identified above are always fixed to the same ranges of R_{ib}. Such questions are beyond the scope of the current study, however, and will be left for future work.

The $R_{ib}-D_{rb}$ relationship presented in Fig. 2 represents boundary layers with a large range of characteristics, bracketed by two quasi-stability-independent states corresponding to fully-coupled ($R_{ib} < 0.03$) and fully-decoupled ($R_{ib} > 1$). Between these two asymptotes is seen a broad transitional regime representing a progressive decoupling of the surface-bounded layer from the overlying atmosphere as the layer bulk stability increases. This three-regime classification of the SBL is similar to that adopted by Mahrt et al. (1998), who used z/L as their stability parameter. The current results show, however, that particularly in the transitional region (centred around the commonly-assumed critical bulk Richardson

number of $R_{ib} \approx 0.2$), the degree of bulk scalar mixing (D_{rb}) exhibits a large variability even within a fixed R_{ib} bin. This is to be expected, given the large range of competing processes operating to influence bulk mixing in the SBL (as discussed in Sect. 1), and it will be seen that a bivariate analysis of key variables in R_{ib}–D_{rb} space is a useful method for further exploration of these processes.

3.2 Interpretation of Position in R_{ib}–D_{rb} Space

Because local turbulent mixing characteristics can change with altitude relative to SBL depth (z/h), the value calculated for R_{ib} depends on the height of the upper measurement. However, D_{rb} can be considered to be a de facto vertical mixing coordinate that is matched to R_{ib}. When $D_{rb} \approx 0$, the layer of interest is completely mixed and the upper measurement height ($z_{\mathrm{m}} = 50$ m) is effectively indistinguishable from the near-surface measurement height (i.e., $z_{\mathrm{m}}/h \to 0$). On the other hand, when $D_{rb} \approx 1$, the surface-bounded layer is decoupled from the atmosphere above and the upper measurement height is completely removed from surface influences (i.e., $z_{\mathrm{m}}/h \to \infty$). This reasoning suggests that a degree of universality should exist in the representation of turbulence quantities in R_{ib}–D_{rb} space, such that changes in the (relative) height of the upper measurement lead to a vertical shift in the position of the maximum point density in the joint frequency distribution (Fig. 2b), but do not affect the shape of distributions of turbulence quantities mapped onto the same space. It should be noted, however, that this "universality" would only be expected to hold for passive scalars that have similar characteristics to radon: in particular, residence/decay times that are long compared with turbulence time scales and minimal diurnal variations in the surface source function.

For the purposes of visually interpreting position in R_{ib}–D_{rb} space, it is useful to imagine an exponential form for the radon profile, defined by its concentrations at the surface and at the upper measurement height:

$$\hat{c} \equiv \frac{C - C_{\mathrm{b}}}{C_{\mathrm{s}} - C_{\mathrm{b}}} = \mathrm{e}^{-z/h_{\mathrm{e}}}, \tag{3a}$$

$$h_{\mathrm{e}} = \frac{-z_{\mathrm{m}}}{\ln\left(1 - D_{rb}\right)}, \tag{3b}$$

where $h_{\mathrm{e}} \equiv \int_0^{\infty} \hat{c}\,\mathrm{d}z$ is the integral length scale calculated using $C(z_{\mathrm{m}})$, C_{s} and C_{b}, assuming the exponential distribution. The distribution of $C_{\mathrm{s}} - C_{\mathrm{b}}$ in R_{ib}–D_{rb} space (not shown) can then be applied to calculate the set of idealized profiles shown in Fig. 3.

Following up the main spine of the joint frequency distribution in Fig. 3 (h → f → c), we see a progression from a well-mixed boundary layer that is much deeper than the tower (Fig. 3h) to a shallow decoupled layer with large radon values very near the surface, dropping sharply to near-background levels at 50 m (Fig. 3c). Off-spine cases also have physical meaning: Fig. 3j (small D_{rb}/large R_{ib}) probably corresponds to a moderately mixed vSBL with depth just above the upper measurement height of 50 m, and Fig. 3a (large D_{rb}/small R_{ib}) includes early evening cases where vertical temperature gradients remain small and radon has only just started to accumulate near the ground. It has been verified that this part of the distribution contains a relatively high proportion of early evening data (not shown).

3.3 Thermodynamic Gradients and External Influences

Figure 4 presents conditional median distributions (CMD) of the bulk thermodynamic gradients in R_{ib}–D_{rb} space. CMDs are formed by calculating the median value of a measured quantity using all hourly data points falling into a particular bivariate grid cell.
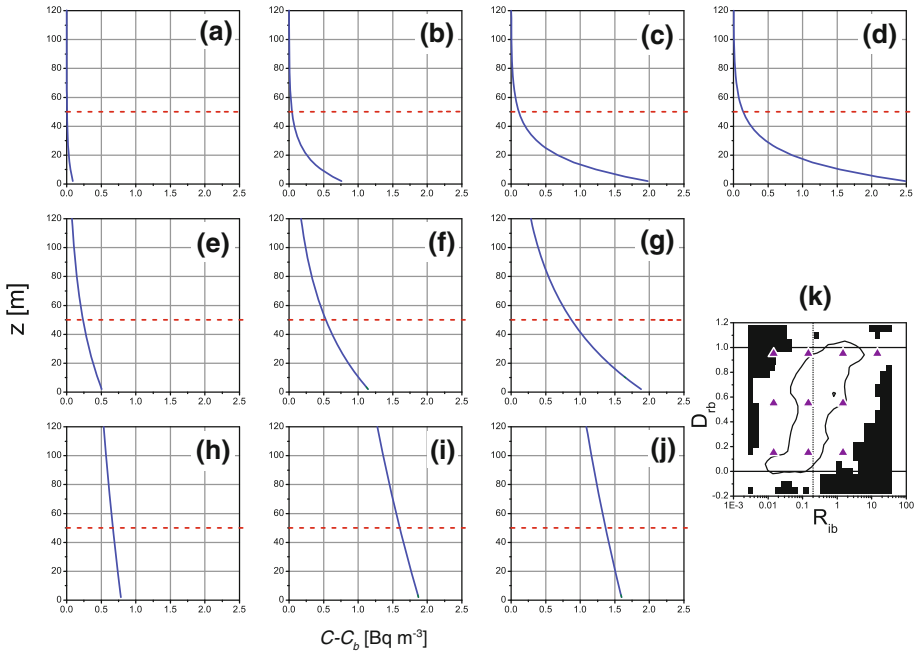
Fig. 3 **a–j** Idealized exponential vertical radon profiles (*solid blue lines*), based on the distribution of $C_s - C_b$ in $R_{ib} - D_{rb}$ space at the positions marked by purple triangles in **k**. *Dashed red lines* indicate the upper measurement height ($z_m = 50$ m). In **k**, grid squares containing less than four data points are masked out in *black*. The *thick black line* corresponds to the 1 % per grid square contour of the $R_{ib} - D_{rb}$ JFD (Fig. 2b)
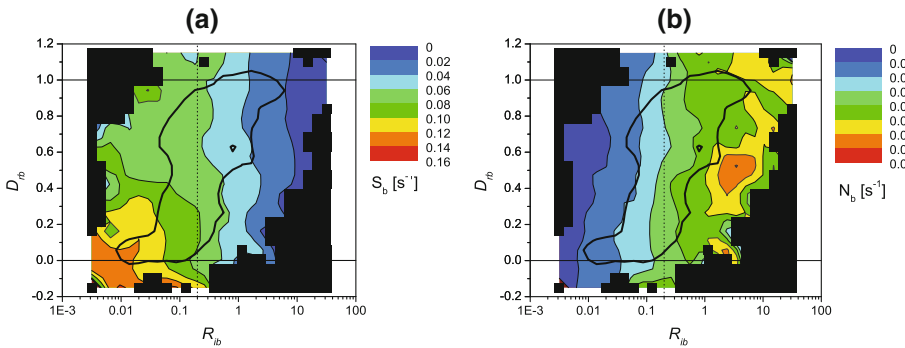

Fig. 4 Conditional median distributions of bulk thermodynamic gradients: **a** wind shear; **b** Brunt–Väisälä frequency

Figure 4a exhibits the expected overall decrease in wind shear (S_b) with increasing stability (R_{ib}). A CMD of the 2-m wind speed (not shown) indicates that low wind speeds (< 0.5 m s^{-1}) are common near the surface when $R_{ib} > 0.3$ for all D_{rb}. At the near-neutral end, however, increasing D_{rb} is linked with decreasing wind shear, so that the highest wind speeds are associated with the smallest values of both R_{ib} and D_{rb}. Figure 5a, which presents the 850-hPa geostrophic winds derived from the Australian Bureau of Meteorology's regional LAPS model (Puri et al. 1998), confirms that low R_{ib}/ low D_{rb} periods tend to be associated
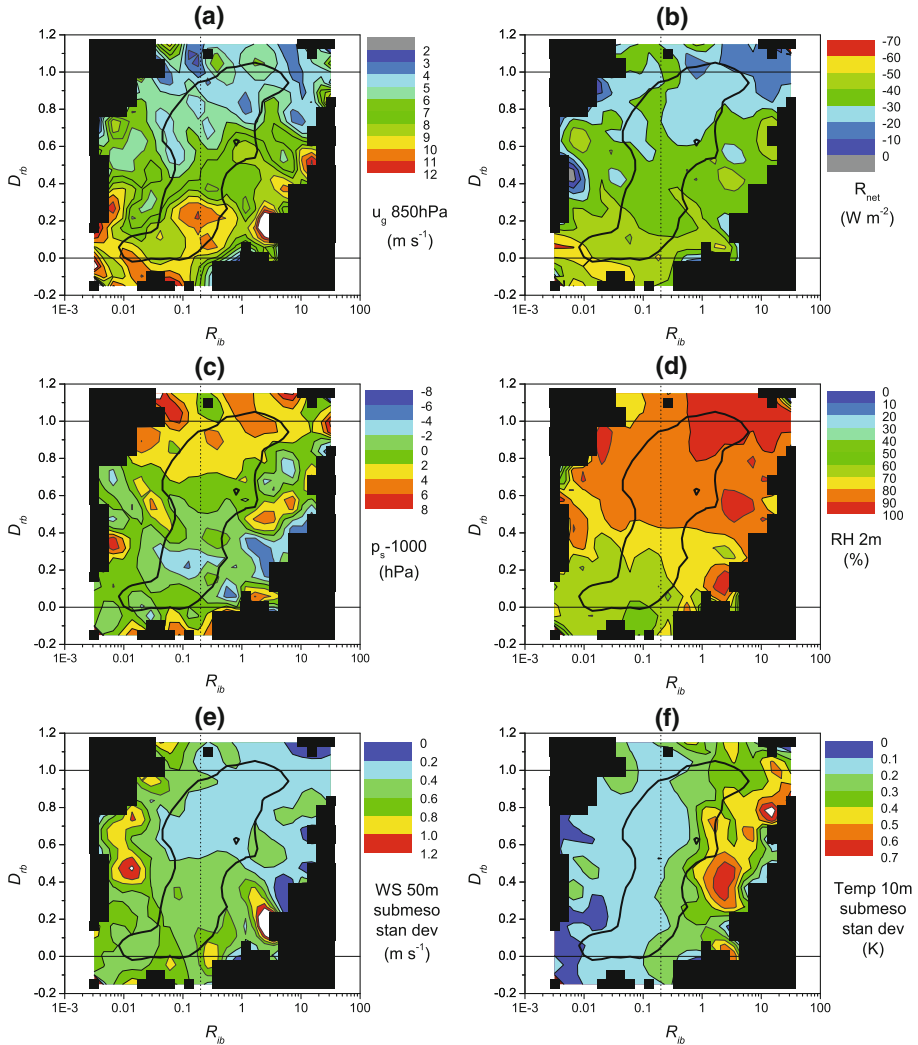
Fig. 5 Indicators of external influences on mixing: **a** 850-Pa geostrophic wind from the LAPS model; **b** net radiation; **c** surface pressure; **d** relative humidity at 2 m; and submeso standard deviations of **e** 50-m wind speed; and **f** 10-m temperature

with a strong "background" pressure gradient driving the wind shear. As discussed in Sect. 3.2, this region of R_{ib}–D_{rb} space is associated with a well-mixed boundary layer that is much deeper than the Lucas Heights tower (c.f. Fig. 3h).

On the other hand, high values of D_{rb} in near-neutral conditions (Fig. 3a or b) are associated with moderate wind speeds, and can occur in the early evening at this site (before the temperature profile has altered appreciably), or in overcast/foggy conditions. Figure 5a–c confirm that geostrophic winds tend to be relatively weak, net radiation tends to be small in magnitude and surface pressures tend to be relatively high in this region of R_{ib}–D_{rb} space.

The bulk temperature gradient (expressed as a Brunt–Väisälä frequency in Fig. 4b) increases uniformly with increasing stability up to a little beyond the critical bulk Richardson

number ($R_{ib} \approx 0.2$–1.0). At higher stabilities ($R_{ib} > 1$), however, a strong variation with D_{rb} is evident. The largest temperature gradients do not correspond to the most decoupled conditions ($D_{rb} \approx 1$), as might be expected, but are instead associated with values of the decoupling index in the range $D_{rb} < 0.7$.

Again, the indicators of external influences shown in Fig. 5 provide us with explanations for these observations. The high R_{ib}/high D_{rb} region of R_{ib}–D_{rb} space tends to be associated with high relative humidity (Fig. 5d) and low net radiation (Fig. 5b), which may indicate the presence of low cloud or thin patchy fog at this ridge-top site (thicker fog tends to occur mainly in the nearby valleys). Together with the possible release of latent heat at the surface by dew formation, this explains the reduced bulk temperature gradients in this part of the distribution. Relatively high surface pressures (Fig. 5c) may indicate that subsidence is acting to promote decoupling. Finally, geostrophic forcing (Fig. 5a) is very small. As will be seen in the next section, these conditions correspond to the smallest turbulence intensities encountered at this site.

The D_{rb} range exhibiting the largest temperature gradients ($D_{rb} < 0.7$) at high stabilities, on the other hand, tends to be associated with relatively large magnitude net radiation values (Fig. 5b) and higher geostrophic winds (Fig. 5a). This suggests clearer nights and the possibility of low-level jets. Such conditions, together with the higher Brunt–Väisälä frequencies, are often associated with the presence of gravity waves and other submeso phenomena that can excite sporadic turbulent mixing (see Sect. 1). In fact, evidence for increased submeso variability in this range is seen in the CMDs of submeso variations of 50-m mean wind speeds and 10-m mean temperatures (Fig. 5e, f). We identify this region of R_{ib}–D_{rb} space as representing a top-down mixing regime.

In summary, the bulk thermodynamic gradients exhibit patterns of variability that are not functions of R_{ib} alone. Different combinations of values for the bulk temperature gradient and wind shear that together correspond to the same value for R_{ib}, map onto distinctly different regions in R_{ib}–D_{rb} space. These regions, which match with particular sets of values for various important indicators of external influences, will be seen below to correspond to vastly different regimes of turbulent mixing in the SBL.

3.4 Distributions of Turbulence Quantities

3.4.1 Variances

Figure 6a shows scatter and binned median/quartile plots of the vertical velocity standard deviation σ_w at 10 m versus bulk Richardson number (calculated across the layer 2–50 m) for all hourly data points. It is immediately seen that at 10-m height there is a strong relationship between turbulence intensity and bulk stability, with the D_{rb}-averaged σ_w values decreasing steeply across a transitional regime from around $0.6 \, \text{m s}^{-1}$ in weakly stable conditions to less than $0.1 \, \text{m s}^{-1}$ in very stable conditions. The transition occurs across two decades of R_{ib} centred around 0.2 with σ_w being relatively R_{ib} independent on either side. These general characteristics of the binned σ_w plot at 10 m (Fig. 6a) match with the three regimes identified in the stability-mixing relationship (see Sect. 3.1 and Fig. 2), and compare well with the velocity variance versus Richardson number relationship observed during the FLOSSII experiment (Fig. 9 in Mahrt and Vickers 2006), as well as results from the Microfronts project (Fig. 1 in Mahrt et al. 1998) and CASES-99 (Fig. 2 in Banta et al. 2007).

In contrast to the 10-m results, σ_w at 50 m (not shown) is more scattered over the whole range of R_{ib}; in Fig. 6b, the median 50-m/10-m σ_w ratio reaches values significantly greater than unity for large R_{ib}. In Fig. 6a, b, the binned results are also split into three categories corresponding to low (-0.1 to 0.2), medium (0.3 to 0.7) and high (0.9 to 1.1) ranges of D_{rb}.
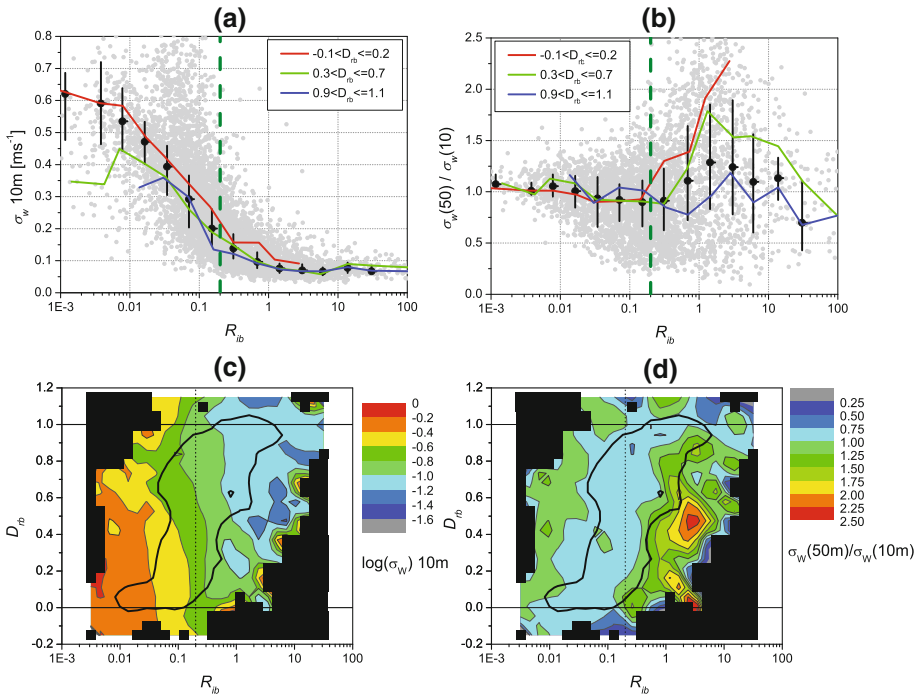
Fig. 6 **a** Median/quartile plot of vertical velocity standard deviation (σ_w) at 10 m in logarithmic R_{ib} bins (*black*), split into three categories corresponding to different ranges of D_{rb} (*red, green, blue*), and scatter plot of hourly values in *grey*; **b** same for ratio of σ_w at 50 m and 10 m; **c** CMD of σ_w at 10 m (note logarithmic colour scale); **d** CMD of ratio of σ_w at 50 and 10 m

At 10 m, the three D_{rb} categories all produce similar plots of σ_w versus R_{ib} (Fig. 6a), whereas in the 50-m/10-m ratio plot the three categories split wide apart after $R_{ib} = 0.2$ (Fig. 6b). In the high D_{rb} category, in which the 50-m measurement level is completely decoupled from the surface, the median σ_w values at 50 m are slightly smaller than those seen at 10 m (ratio < 1). In contrast, the two lower D_{rb} categories both capture 50-m σ_w values that are significantly higher than those found at 10 m (ratio ≫ 1) for a similar range of R_{ib}. In fact, D_{rb} variability accounts for the majority of the increased scatter at high R_{ib} values in the 50-m σ_w data.

Figure 6c shows a CMD plot of σ_w at 10 m; the highest values of σ_w at 10 m are found in the low R_{ib}/low D_{rb} sector and the lowest in the high R_{ib}/high D_{rb} sector, with the remaining areas showing intermediate values. A CMD plot of the ratio of σ_w at 50 m to σ_w at 10 m (Fig. 6d) furthermore reveals that σ_w values at 50 m are similar or only slightly less than those at 10 m all along and to the left of the main spine of the JFD (see also Fig. 6b). As discussed in Sect. 3.2 (see Fig. 3), for near-neutral R_{ib} and small D_{rb} the SBL is likely to be significantly deeper than the height of the tower and we should not expect significant vertical variations of turbulence quantities. Furthermore, as low R_{ib}/high D_{rb} cases tend to occur in the early evening, it may be that high σ_w values at 50 m correspond either to mixing near the top of a growing new stable layer, or to remnant decaying turbulence from the previous afternoon.

In the narrow part of the high R_{ib}/high D_{rb} sector centred on $D_{rb} = 1$, where the lowest σ_w values are found at 10 m (Fig. 6c), the 50-m/10-m ratio is close to or even slightly less than
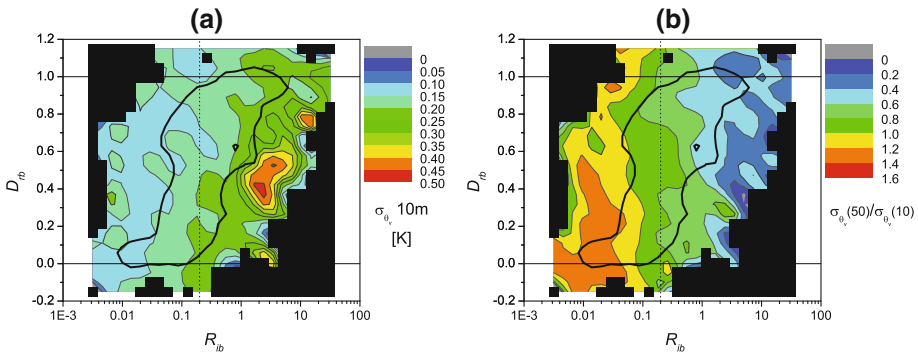
Fig. 7 CMDs of: **a** virtual (sonic) temperature standard deviation ($\sigma_{\theta v}$) at 10 m; **b** ratio of $\sigma_{\theta v}$ at 50 and 10 m

unity in Fig. 6d. The 50-m σ_w values in this region are the smallest encountered in this dataset, confirming that this region of R_{ib}–D_{rb} space corresponds to a vSBL topped with a "quiescent layer" (Banta et al. 2007). In strong contrast, much higher ratios are found for $D_{rb} < 0.7$ at high R_{ib}. In the range $0.4 < D_{rb} < 0.6$, σ_w at 50 m can be 2.5 times larger than σ_w at 10 m for $R_{ib} > 1$ (Fig. 6d). This corresponds precisely to the region of maximum Brunt–Väisälä frequency in Fig. 4b, strongly suggesting a top-down mixing regime. Increased turbulence intensities aloft in moderately and very stable conditions have been found by others to be associated with the presence of low-level jets (Conangla and Cuxart 2006; Conangla et al. 2008) that can excite gravity wave and other sub-meso disturbances.

In Fig. 7, we present standard deviations of sonic potential temperature (10-m values and 50-m/10-m ratios), noting that sonic potential temperature is closely related to virtual potential temperature (Kaimal and Gaynor 1991), θ_v. Through the weakly stable regime, the 10-m $\sigma_{\theta v}$ stays approximately constant with low values around 0.14 K (Fig. 7a). Significant $\sigma_{\theta v}$ values require vertical motions in the presence of a temperature gradient, and at low R_{ib} values temperature gradients are very small (Fig. 4b). Through the transitional regime, the temperature gradient increases but vertical motions decrease, resulting in $\sigma_{\theta v}$ values that only slowly increase (Fig. 7a). Little D_{rb} variation is evident, other than a slight trend towards smaller $\sigma_{\theta v}$ at high D_{rb} values.

For high R_{ib} values ($R_{ib} > 1$), however, $\sigma_{\theta v}$ at 10 m varies strongly with D_{rb} (Fig. 7a). For values of D_{rb} above 0.8, σ_θ at 10 m remains relatively small, presumably due to the extremely low turbulence levels (see discussion in previous section). However, for $D_{rb} < 0.7$, $\sigma_{\theta v}$ values become large. In the range $0.4 < D_{rb} < 0.6$, median $\sigma_{\theta v}$ values at 10 m reach 0.5 K, following a pattern similar to, and consistent with, that of the high vertical temperature gradients found in that range (Fig. 4b).

For low R_{ib}, $\sigma_{\theta v}$ values are similar or even increase slightly from 10 to 50 m (ratio 1.0–1.2 in Fig. 7b). As R_{ib} increases, however, the 50-m/10-m $\sigma_{\theta v}$ ratio decreases steadily and uniformly across D_{rb} values, reaching values around 0.3 or smaller above $R_{ib} \approx 1$. This is consistent with progressively larger temperature gradients near the surface as R_{ib} increases.

3.4.2 Fluxes and Intermittency

The CMD of the 10-m momentum flux, expressed as a friction velocity (u_*), reduces smoothly with increasing R_{ib} (Fig. 8a). Little D_{rb} variation is evident, except in near-neutral conditions where u_* decreases with increasing D_{rb} consistent with decreasing wind shear (Fig. 4a).
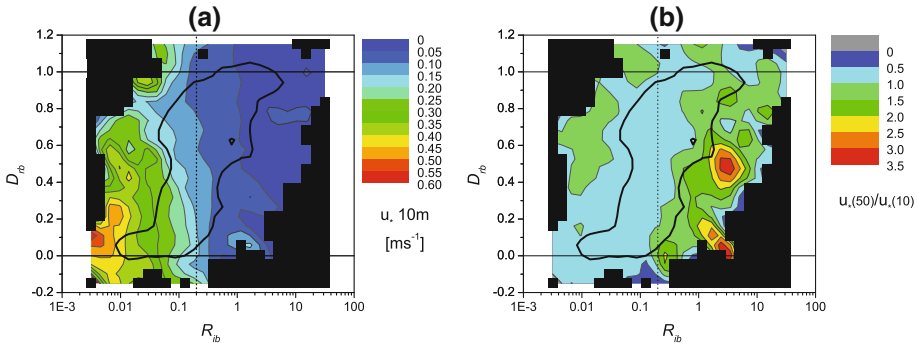
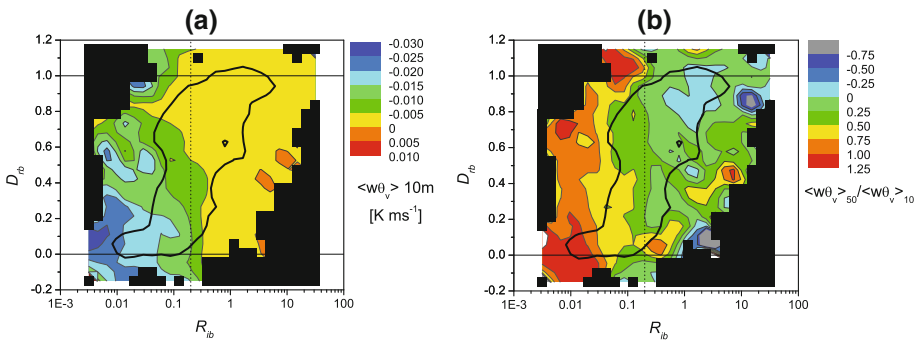**Fig. 8** CMDs of: **a** friction velocity (u_*) at 10 m; **b** ratio of u_* at 50 and 10 m

Fig. 9 CMDs of: **a** kinematic virtual (sonic) heat flux ($\langle w\theta_v \rangle$) at 10 m; **b** ratio of $\langle w\theta_v \rangle$ at 50 and 10 m

u_* reduces slightly with height throughout much of the present dataset, with 50-m/10-m u_* ratios around 0.8 along the spine of the JFD (Fig. 8b), except in the $R_{ib} > 1/D_{rb} < 0.7$ region where u_* at 50 m can be very significantly (up to 3.5 times) *larger* than u_* at 10 m.

As has been noted previously, it is not surprising to find little change from 10 to 50 m in the low R_{ib}/low D_{rb} region. However, the fact that the 50-m/10-m u_* ratio was often significantly greater than unity and rarely <0.8 for $R_{ib} > 0.2$ in the present dataset indicates that nighttime mechanical mixing is often driven from above at this site. An increase of wind stress with height in very stable conditions has been noted by others and attributed to mixing driven by elevated sources including low-level jets (Forrer and Rotach 1997; Ohya et al. 1997; Ohya 2001; Ha and Mahrt 2001; see also discussion in Mahrt 1999). Even in the high R_{ib}/high D_{rb} region the ratio tended to remain in the range 0.8–1.0 (Fig. 8b), contrasting with vSBL topped with quiescent layers encountered in the CASES-99 experiment over flat grassland (Banta et al. 2007) where u_* values fell dramatically with altitude.

Figure 9 presents CMDs of 10-m sonic temperature fluxes and 50-m/10-m flux ratios; these covariances correspond approximately to kinematic virtual heat (buoyancy) fluxes, $\langle w\theta_v \rangle$. Despite the small temperature gradients, heat fluxes at 10 m (Fig. 9a) are largest in magnitude in the low R_{ib}/low D_{rb} region, due to the strong vertical motions present. As R_{ib} values increase and turbulence levels fall through the transition regime, however, the heat flux is rapidly suppressed, reaching small values for $R_{ib} > 0.3$. Heat fluxes at 50 m are similar to those at 10 m in near-neutral conditions (ratio ≈ 1 in Fig. 9b), but the ratio decreases rapidly to near-zero values for $R_{ib} > 0.2$. Above $D_{rb} = 0.7$ at high R_{ib}, 50-m fluxes and 50-m/10-m
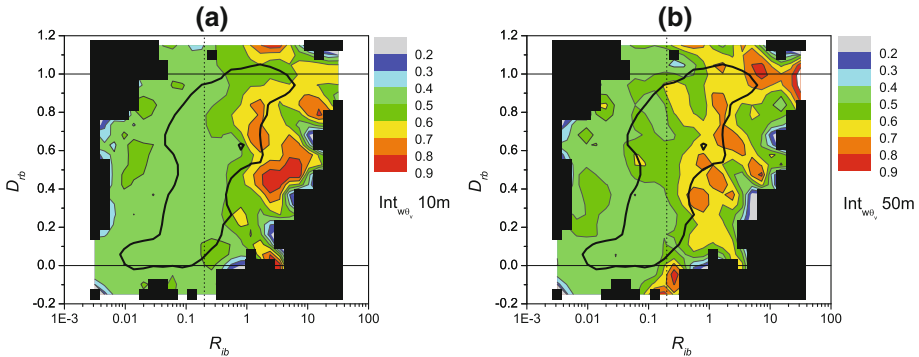
Fig. 10 CMDs of heat flux intermittency factor at **a** 10 m and **b** 50 m

flux ratios are indistinguishable from zero to the accuracy of these measurements. Below $D_{rb} = 0.7$, the heat-flux ratio is small and variable but remains mainly positive.

Integrating the distribution in Fig. 9a across all D_{rb} values (not shown), we find that the maximum (negative) virtual heat flux, corresponding to the point of balance between small temperature fluctuations in near-neutral conditions and suppressed vertical motions as the stratification becomes more stable (Derbyshire 1990; Malhi 1995; Mahrt et al. 1998), occurs at around $R_{ib} = 0.01$ in the present dataset. This roughly coincides with the boundary between the weakly stable and the transitional regimes. When the heat flux is re-plotted against binned values of the Obukhov stability parameter (not shown), the maximum value is found to be at around $z/L = 0.4$, which compares well with the results of Mahrt et al. (1998).

The complete collapse of heat fluxes at 50 m in the high R_{ib}/high D_{rb} region (Fig. 9b) compares well with cases of the vSBL topped with a quiescent layer seen in the CASES-99 experiment (Mahrt and Vickers 2002; Banta et al. 2007). In the high R_{ib}/low D_{rb} region, which we have interpreted as a "top-down" intermittent mixing regime, this extreme attenuation of heat fluxes with height is less pronounced. However, in this dataset we do not encounter the significant *increases* in heat-flux magnitudes with height that have been seen by others in upside-down cases (e.g. Mahrt 1985; Ohya et al. 1997). This contrasts with our results for u_*, discussed above, and may indicate that "top-down" mixing tends to be more efficient in transporting momentum than heat at this site, a fact that is perhaps related to the types of submeso motions generated by the complex topography. It is interesting to note that, in the wind-tunnel study of Ohya (2001), the addition of surface roughness elements was found to remove the vertically increasing heat flux they had observed over smooth surfaces (Ohya et al. 1997) in the most stable cases.

Finally, the intermittency of the virtual heat flux, defined here as the fraction of 2-min sonic temperature fluxes that are larger (more positive) than the mean flux in each 1-h record (average of 30×2-min fluxes), is presented in Fig. 10. Intermittency remains close to 0.5 for $R_{ib} < 0.2$ at both levels, but starts to increase for larger R_{ib}. At $z = 50$ m, the increase starts earlier (at lower R_{ib} values) and is widespread across all values of D_{rb}, whereas at $z = 10$ m the increased values are concentrated mainly in the range $0.3 < D_{rb} < 0.9$. The largest intermittencies are found in the range $0.4 < D_{rb} < 0.6$ at $z = 10$ m, where their values exceed 0.8. Values of various intermittency measures that increase with increasing stability and decrease in intensity with height have been reported by others (e.g. Mahrt 1998, 2010b). Nappo (1991) suggests that, in very stable conditions, the major portion of heat, momentum

and mass transfer near the surface is accomplished during intermittent episodes of strong mixing leading to temporary breakdown of the stability profile.

3.5 Discussion

With the exception of temperature variances, all the turbulence quantities presented change rapidly with increasing R_{ib} through the transitional regime, and then change much more slowly and become highly variable in the very stable regime. This behaviour is similar to that reported by Mahrt et al. (1998) and others, and it is clear from the current study that a significant part of the variability seen at high R_{ib} is due to changes in the degree of decoupling of the surface-bounded very stable boundary layer (vSBL) from the residual layer above. Large changes in decoupling can occur for a constant value of R_{ib}, depending critically upon the particular combination of the bulk wind shear and bulk Brunt–Väisälä frequency present, which in turn are related to a range of external parameters, including net radiation, geostrophic forcing and surface pressure (as discussed in Sect. 3.3).

The extremely low turbulence intensities (σ_w) and temperature variances at $z = 50\,\mathrm{m}$ compared with $z = 10\,\mathrm{m}$, found when the radon decoupling index is near unity ($D_{rb} \approx 1$) at high bulk Richardson numbers ($R_{ib} \approx 1$–10), identifies this region of the R_{ib}–D_{rb} distribution with the "quiescent layer" as defined by Banta et al. (2007). The fact that 50-m momentum and heat fluxes are also found to be negligibly small in this region further confirms that the presence of this layer indicates that the atmosphere above is completely isolated from the shallow ($\ll 50\,\mathrm{m}$) vSBL below. In terms of external influences on the turbulent mixing, this fully decoupled shallow vSBL tends to occur when geostrophic forcing (u_g) is small and surface pressure is high. Quiescent conditions in this dataset tend to be associated with relatively small net radiation magnitudes and high humidities, which we take to indicate the presence of low cloud, patchy fog and the possibility of dew formation at the surface. This appears to conflict with the expectation that the weakest turbulence occurs in clear-sky conditions, suggesting that radiative effects may not always be the dominant factor in determining turbulence levels at low wind speeds. The consequence of this important observation is that quiescent layers do not necessarily occur when the temperature gradients are largest (clear skies). The largest Brunt–Väisälä frequencies are in fact associated with smaller values of the decoupling index ($D_{rb} < 0.7$) in this dataset, indicating the outcome of enhanced mixing. The presence of strongly stratified flows and low-level jets is known to be conducive to the generation of gravity waves and other submeso phenomena that can excite sporadic turbulent mixing (see discussion in Sect. 1). Strong evidence confirming the identification of this region of the R_{ib}–D_{rb} distribution as a top-down mixing regime has been seen in enhanced turbulence levels, fluxes and submeso activity at $z = 50\,\mathrm{m}$, and high temperature variances and heat-flux intermittencies at $z = 10\,\mathrm{m}$.

It is interesting to note that, in this dataset, weak geostrophic forcing, higher surface pressures and the occurrence of low cloud, patchy fog or dew tend to be associated with decoupled conditions *irrespective* of the value of the bulk Richardson number. This may in part be attributable to the site's location on a ridge top. Such locations are susceptible to slow drainage flows into nearby valleys at night in light winds and subsidence conditions, thereby preventing the formation of a deep SBL on the high ground (Price et al. 2011).

4 Summary and Conclusions

The aim of this study was to characterize the bulk properties (vertically-integrated behaviour) of the SBL at the Lucas Heights site for a range of bulk stabilities (R_{ib}), using the radon-based

decoupling index D_{rb} as an independent measure of the degree of decoupling of the upper (50 m) measurement level from the surface-bounded turbulent mixed layer.

The general characteristic of the $R_{ib}-D_{rb}$ relationship is a progressive increase in decoupling of the surface-bounded layer from the atmosphere above as R_{ib} increases, centred around the commonly used critical Richardson number $R_{ib}(crit) = 0.2$. However, within this general relationship D_{rb} exhibits a large range of values for any given R_{ib}, due to a number of competing processes operating to influence bulk mixing under different conditions. A bivariate analysis of key variables in $R_{ib}-D_{rb}$ space was found to be a useful method for exploration of these processes.

The decoupling index D_{rb} provides an unbiased quantification of the layer-integrated outcome of the turbulent mixing process. It is not affected by temporal or geographic variations in the surface flux within the measurement footprint, and does not influence the thermodynamic processes determining the evolution of the SBL. Furthermore, D_{rb} can be considered to be a de facto normalized vertical mixing coordinate that is matched with R_{ib} in a way that suggests a degree of universality in the representation of turbulence quantities in $R_{ib}-D_{rb}$ space. For example, changes in the height of the upper measurement are expected to lead only to a vertical shift in the position of the maximum point density in the joint frequency distribution in $R_{ib}-D_{rb}$ space, but are not expected to affect the conditional median distributions (CMD) of key turbulence quantities mapped onto the same space. Likewise, whereas the distribution of cases within the JFD would be expected to change somewhat from site to site, the characteristic patterns seen in the CMDs might not. Such hypotheses cannot be tested until similar datasets are available from other sites, however. It should also be remembered that this "universality" would only be expected to hold for passive scalars with similar characteristics to radon (long residence/decay times and minimal temporal variations in the surface source function).

The observed bivariate distributions of turbulence quantities match well with those of the bulk thermodynamic gradients and various indicators of external influences. This leads to consistent and strong interpretations of various significant regions in $R_{ib}-D_{rb}$ space, which seems to support our universality hypothesis. It is therefore a reasonable proposition to associate these well-defined regions with archetypal SBL regimes. Figure 11 represents an attempt to postulate such an association, based on the evidence presented in this study. Within this model, we identify five major regions of $R_{ib}-D_{rb}$ space and associate them with the following set of SBL archetypes:

1. *The near-neutral deep SBL* ($R_{ib} < 0.03$, $D_{rb} < 0.4$; 7.6 % of cases) is a well-mixed layer that is much deeper than the 50-m Lucas Heights tower. A strong background synoptic pressure gradient drives significant wind shear in the lower atmosphere, which overrides any effects of longwave surface cooling associated with clear skies.

2. *The near-neutral shallow SBL* ($R_{ib} < 0.03$, $D_{rb} \geq 0.4$; 3.4 % of cases) is a moderately mixed layer that is relatively shallow (<50 m if $D_{rb} \approx 1$). Although a weak synoptic pressure gradient drives only a moderate wind shear, prevailing thermal conditions have precluded the development of a vertical temperature gradient. These include overcast/foggy skies, and early evening conditions in which the sensible heat flux and radiation divergence have not yet acted long enough to alter the temperature profile appreciably and radon has only just started to accumulate near the ground.

3. *The transitional SBL* ($0.03 \leq R_{ib} < 1$; 66.4 % of cases) is a moderately mixed layer, probably of depth 50–80 m at this site, with a relatively small wind shear and a developing temperature gradient. In this state, small changes in the driving wind shear and/or temperature gradient can lead quickly to changes in turbulent mixing and fluxes. The
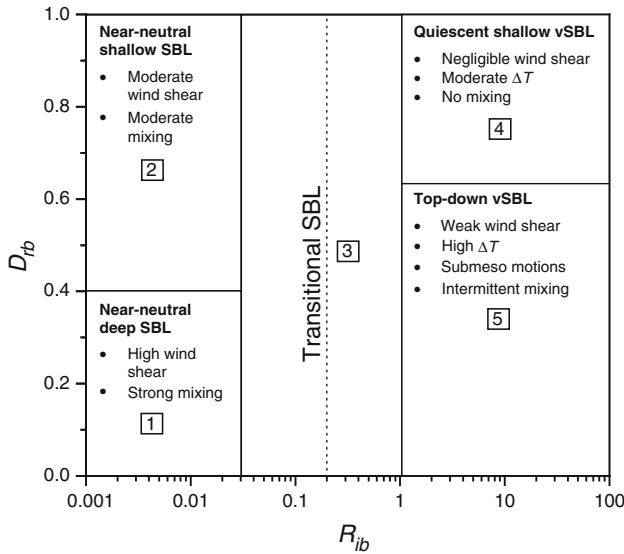
Fig. 11 SBL archetypes in R_{ib}–D_{rb} space (see text for discussion)

boundary layer remains continuously turbulent and has not yet started to show strong signs of turbulence decay and intermittency. Turbulence levels and fluxes tend to reduce with height, and the layer becomes progressively thinner and decoupled as the bulk Richardson number increases. This archetype has sometimes been called the "traditional boundary layer" (e.g. Mahrt and Vickers 2002).

4. *The shallow vSBL topped with a quiescent layer* ($R_{ib} \geq 1$, $D_{rb} \geq 0.7$; 14.7 % of cases) is a very shallow ($\ll 50$ m) completely decoupled layer with negligible wind shear (no pressure gradient), temperature gradients that are strong but may be limited by the presence of low cloud, patchy fog or dew, and weak vertical motions that have not been enhanced by the presence of low-level jets and submeso motions. This boundary layer is characterized by vanishing turbulence levels and fluxes with height, and resembles the "extremely weak mixing" cases of Mahrt and Vickers (2006) and the "quiescent" cases of Banta et al. (2007). This SBL archetype is likely to be associated with the maximum build-up of contaminants at the surface and possibly slow drainage flows down into the nearby valleys at this ridge-top site.

5. *The top-down vSBL* ($R_{ib} \geq 1$, $D_{rb} < 0.7$; 7.9 % of cases) is a weakly to moderately mixed layer with clear skies and very strong temperature gradients. Small but not negligible wind shear, submeso motions and low-level jets aloft drive intermittent top-down turbulence events that mix momentum and temperature downwards towards the surface.

In general, the results of this study suggest that the introduction of a decoupling index based on a simple passive scalar can yield valuable information about the turbulent mixing process in the SBL that cannot be gained directly from a single bulk thermodynamic stability parameter. Large variability of scaled turbulence quantities such as the drag coefficient at high bulk Richardson numbers has been attributed to a loss of applicability or accuracy of the scaling variable as turbulence degenerates and becomes more intermittent and influenced by submeso motions (Mahrt 2010b). The results of the current study emphasize this viewpoint and suggest that for $R_{ib} > 1$ different turbulence regimes may occur for the same R_{ib} depending on the

particular combination of values for N_b and S_b. In this study, the highest N_b values tend to be associated with submeso activity and upside-down mixing, which may indicate an important role for gravity waves and other wave-like phenomena in providing energy required for sporadic mixing at this site. It is known that the submeso energy is generally greater in complex terrain (Nappo 1991; Vickers and Mahrt 2006). It is also possible that, in a fashion similar to semi-open forest canopies, the irregular roughness elements in the vicinity of the Lucas Heights tower can occasionally induce gravity waves in very stable conditions near the surface that have phase angles significantly different from $\pm 90°$ and can therefore contribute to fluxes of momentum and heat (Lee et al. 1996, 1997). In complex topography, Acevedo and Fitzjarrald (2003) found that temperature recoupling between regional stations at different altitudes occurred more frequently as wind speeds or cloud fractions increased. Our results concur with their wind-speed finding, but suggest that in very stable conditions (high R_{ib}) low cloud, patchy fog or dew formation may actually be associated with *stronger* decoupling if the wind speed is very low. This is because under such circumstances mechanical forcing is completely suppressed and temperature gradients do not increase sufficiently to initiate gravity wave activity that leads to top-down mixing.

Future studies are planned to focus on the behaviour of scaled variables in $R_{ib}-D_{rb}$ space, diurnal variability of decoupling and stability, and further exploration of the site-dependence of these results.

References

Acevedo OC, Fitzjarrald DR (2003) In the core of the night—effects of intermittent mixing on a horizontally heterogeneous surface. Boundary-Layer Meteorol 106:1–33

Banta RM, Mahrt L, Vickers D, Sun J, Balsley BB, Pichugina YL, Williams EL (2007) The very stable boundary layer on nights with weak low-level jets. J Atmos Sci 64:3068–3090

Businger JA (1973) Turbulent transfer in the atmospheric surface layer. In: Haugen DA (ed) Workshop on micrometeorology. American Meteorological Society, Boston, pp 67–100

Butterweck G, Reineking A, Kesten J, Porstendorfer J (1994) The use of the natural radioactive noble gases radon and thoron as tracers for the study of turbulent exchange in the atmospheric boundary layer—case study in and above a wheat field. Atmos Environ 28:1963–1969

Chambers S, Williams AG, Zahorowski W, Griffiths A, Crawford J (2011) Separating remote fetch and local mixing influences on vertical radon measurements in the lower atmosphere. Tellus 63B:843–859

Conangla L, Cuxart J (2006) On the turbulence in the upper part of the low-level jet: an experimental and numerical study. Boundary-Layer Meteorol 118:379–400

Conangla L, Cuxart J, Soler MR (2008) Characterisation of the nocturnal boundary layer at a site in northern Spain. Boundary-Layer Meteorol 128:255–276

Cuxart J, Yagüe C, Morales G, Terradellas E, Orbe J, Calvo J, Fernández A, Soler MR, Infante C, Buenestado P, Espinalt A, Joergensen HE, Rees JM, Vilà J, Redondo JM, Cantalapiedra IR, Conangla L (2000) Stable atmospheric boundary-layer experiment in Spain (SABLES 98): a report. Boundary-Layer Meteorol 96:337–370

Cuxart J, Holtslag AAM, Beare RJ, Bazile E et al (2006) Single-column model intercomparison for a stably stratified atmospheric boundary layer. Boundary-Layer Meteorol 118:273–303

Derbyshire SH (1990) Nieuwstadt's stable boundary Layer revisited. Q J R Meteorol Soc 116:127–158

Druilhet A, Guedalia D, Fontan J (1980) Use of natural radioactive tracers for the determination of vertical exchanges in the planetary boundary layer. In: Gesell TF, Lowder WM (eds) Natural radiation environment III, Houston, US-DOE CONF-780422, vol 1, pp 226–241

Forrer J, Rotach MW (1997) On the turbulence structure in the stable boundary layer over the Greenland ice sheet. Boundary-Layer Meteorol 85:111–136

Gogolak CV, Beck HL (1980) Diurnal variations of radon daughter concentrations in the lower atmosphere. In: Gesell TF, Lowder WM (eds) Natural radiation environment III, Houston, US-DOE CONF-780422, vol 1, pp 259–280

Griffiths AD, Zahorowski W, Element A, Werczynski S (2010) A map of radon flux at the Australian land surface. Atmos Chem Phys 10:8969–8982

Ha KJ, Mahrt L (2001) Simple inclusion of z-less turbulence within and above the modeled nocturnal boundary layer. Mon Weather Rev 129:2136–2143

Ha KJ, Mahrt L (2003) Radiative and turbulent fluxes in the nocturnal boundary layer. Tellus 55A:317–327

Holtslag AAM, Nieuwstadt FTM (1986) Scaling the atmospheric boundary layer. Boundary-Layer Meteorol 36:201–209

Hosler CR (1969) Vertical diffusivity from radon profiles. J Geophys Res 74:7018–7026

Howell JF, Sun J (1999) Surface-layer fluxes in stable conditions. Boundary-Layer Meteorol 90:495–520

Hunt JCR, Kaimal JC, Gaynor JE (1985) Some observations of turbulence structure in stable layers. Q J R Meteorol Soc 111:793–815

Israelsson S (1978) Meteorological influences on atmospheric radioactivity and its effects on the electrical environment. In: Gesell TF, Lowder WM (eds) Natural radiation environment III, Houston, US-DOE CONF-780422, vol , pp 210–225

Kaimal JC, Gaynor JE (1991) Another look at sonic thermometry. Boundary-Layer Meteorol 56:401–410

King JC, Mobbs SD, Darby MS, Reeds JM (1987) Observations of internal gravity waves in the lower troposphere at Halley, Antarctica. Boundary-Layer Meteorol 39:1–14

Klipp CL, Mahrt L (2004) Flux-gradient relationship, self-correlation and intermittency in the stable boundary layer. Q J R Meteorol Soc 130:2087–2103

Lambert G, Polian G, Sanak J, Ardouin B, Buisson A, Jegou A, Le Roulley JC (1982) Cycle du radon et de ses descendants: application à l'étude des échanges troposphère-stratosphère. Ann Géophys 38:497–531

Lee X, Black TA, Den Hartog G, Neumann HH, Nesic Z, Olejnik J (1996) Carbon dioxide exchange and nocturnal processes over a mixed deciduous forest. Agric For Meteorol 81:13–29

Lee X, Neumann HH, Den Hartog G, Fuentes JD, Black TA, Mickle RE, Yang PC, Blanken PD (1997) Observation of gravity waves in a boreal forest. Boundary-Layer Meteorol 84:383–398

Liu SC, McAfee JR, Cicerone RJ (1984) Radon-222 and tropospheric vertical transport. J Geophys Res 89:7291–7297

Mahrt L (1985) Vertical structure and turbulence in the very stable boundary layer. J Atmos Sci 42:2333–2349

Mahrt L (1998) Stratified atmospheric boundary layers and breakdown of models. Theoret Comput Fluid Dyn 11:263–279

Mahrt L (1999) Stratified atmospheric boundary layers. Boundary-Layer Meteorol 90:375–396

Mahrt L (2010a) Common microfronts and other solitary events in the nocturnal boundary layer. Q J R Meteorol Soc 136:1712–1722

Mahrt L (2010b) Variability and maintenance of turbulence in the very stable boundary layer. Boundary-Layer Meteorol 135:1–18

Mahrt L (2011) The near-calm stable boundary layer. Boundary-Layer Meteorol 140:343–360

Mahrt L, Vickers D (2002) Contrasting vertical structures of nocturnal boundary layers. Boundary-Layer Meteorol 105:351–363

Mahrt L, Vickers D (2006) Extremely weak mixing in stable conditions. Boundary-Layer Meteorol 119:19–39

Mahrt L, Sun J, Blumen W, Delany T, Oncley S (1998) Nocturnal boundary-layer regimes. Boundary-Layer Meteorol 88:255–278

Mahrt L, Vickers D, Nakamura R, Soler MR, Sun JL, Burns S, Lenschow DH (2001) Shallow drainage flows. Boundary-Layer Meteorol 101:243–260

Malhi YS (1995) The significance of the dual solutions for heat fluxes measured by the temperature-fluctuation method in stable conditions. Boundary-Layer Meteorol 74:389–396

Nappo CJ (1991) Sporadic breakdown of stability in the PBL over simple and complex terrain. Boundary-Layer Meteorol 54:69–87

Nieuwstadt FTM (1984) The turbulent structure of the stable nocturnal boundary layer. J Atmos Sci 41:2202–2216

Ohya Y (2001) Wind-tunnel study of atmospheric stable boundary layers over a rough surface. Boundary-Layer Meteorol 98:57–82

Ohya Y, Neff DE, Meroney RN (1997) Turbulence structure in a stratified boundary layer under stable conditions. Boundary-Layer Meteorol 83:139–161

Ohya Y, Nakamura R, Uchida T (2008) Intermittent bursting of turbulence in a stable boundary layer with low-level jet. Boundary-Layer Meteorol 126:349–363

Pearson JE, Moses H (1966) Atmospheric radon-222 concentration variation with height and time. J Appl Meteorol 5:175–181

Poulos G, Blumen W, Fritts D, Lundquist J, Sun J, Burns S, Nappo C, Banta R, Newsom R, Cuxart J, Terradellas E, Balsley B, Jensen M (2002) CASES-99: a comprehensive investigation of the stable nocturnal boundary layer. Bull Am Meteorol Soc 83:555–581

Price JD, Vosper S, Brown A, Ross A, Clark P, Davies F, Horlacher V, Claxton B, McGregor JR, Hoare JS, Jemmett-Smith B, Sheridan P (2011) COLPEX—field and numerical studies over a region of small hills. Bull Am Meteorol Soc 92:1636–1650

Puri K, Dietachmayer GS, Mills GA, Davidson NE, Bowen RA, Logan LW (1998) The new BMRC Limited Area Prediction System, LAPS. Aust Meteorol Mag 47:203–223

Smedman AS (1988) Observations of a multi-level turbulence structure in a very stable atmospheric boundary layer. Boundary-Layer Meteorol 44:231–253

Sorbjan Z (2006a) Local structure of turbulence in stably stratified boundary layers. J Atmos Sci 63:1526–1537

Sorbjan Z (2006b) Comments on 'Flux-gradient relationship, self-correlation and intermittency in the stable boundary layer'. Q J R Meteorol Soc 132:1371–1373

Sorbjan Z (2008) Local scales of turbulence in the stable boundary layer. Boundary-Layer Meteorol 127:261–271

Sorbjan Z, Grachev AA (2010) An evaluation of the flux–gradient relationship in the stable boundary layer. Boundary-Layer Meteorol 135:385–405

Sun JL, Burns SP, Delany AC, Oncley SP, Horst TW, Lenschow DH (2003) Heat balance in the nocturnal boundary layer during CASES-99. J Appl Meteorol 42:1649–1666

Sun J, Lenschow DH, Burns SP, Banta RM, Newsom RK, Coulter R, Frasier S, Ince T, Nappo C, Balsley BB, Jensen M, Mahrt L, Miller D, Skelly B (2004) Atmospheric disturbances that generate intermittent turbulence in nocturnal boundary layers. Boundary-Layer Meteorol 110:255–279

Sun J, Mahrt L, Banta RM, Pichugina YL (2012) Turbulence regimes and turbulence intermittency in the stable boundary layer during CASES-99. J Atmos Sci 69:338–351

Turekian KK, Nozaki Y, Benninger LK (1977) Geochemistry of atmospheric radon and radon products. Ann Rev Earth Planet Sci 5:227–255

Ussler WI, Chanton JP, Kelley CA, Martens CS (1994) Radon 222 tracing of soil and forest canopy trace gas exchange in an open canopy boreal forest. J Geophys Res 99:1953–1963

Van de Wiel BJH, Ronda RJ, Moene AF, De Bruin HAR, Holtslag AAM (2002a) Intermittent turbulence and oscillations in the stable boundary layer over land. Part I: a bulk model. J Atmos Sci 59:942–958

Van de Wiel BJH, Moene AF, Ronda RJ, De Bruin HAR, Holtslag AAM (2002b) Intermittent turbulence and oscillations in the stable boundary layer over land. Part II: a system dynamics approach. J Atmos Sci 59:2567–2581

Van de Wiel BJH, Moene AF, Hartogensis OK, De Bruin HAR, Holtslag AAM (2003) Intermittent turbulence in the stable boundary layer over land. Part III: a classification for observations during CASES-99. J Atmos Sci 60:2509–2522

Vickers D, Mahrt L (2003) The cospectral gap and turbulent flux calculations. J Atmos Ocean Tech 20:660–672

Vickers D, Mahrt L (2006) A solution for flux contamination by mesoscale motions with very weak turbulence. Boundary-Layer Meteorol 118:431–447

Wilkening MH, Clements WE (1975) Radon-222 from the ocean surface. J Geophys Res 80:3829–3830

Williams AG, Zahorowski W, Chambers SD, Griffiths A (2011) The vertical distribution of radon in clear and cloudy daytime terrestrial boundary layers. J Atmos Sci 68:155–174

Zilitinkevich S, Elperin T, Kleeorin N, Rogachevskii I, Esau I, Mauritsen T, Miles M (2008) Turbulence energetics in stably stratified geophysical flows: strong and weak mixing regimes. Q J R Meteorol Soc 134:793–799